Deep learning virtual Zernike phase contrast imaging for singlet microscopy

Cite as: AIP Advances **11**, 065311 (2021); https://doi.org/10.1063/5.0053946
Submitted: 13 April 2021 • Accepted: 16 May 2021 • Published Online: 07 June 2021

Yinxu Bian, Yannan Jiang, Weijie Deng, et al.

Deep learning virtual Zernike phase contrast imaging for singlet microscopy

Cite as: AIP Advances 11, 065311 (2021); doi: 10.1063/5.0053946
Submitted: 13 April 2021 • Accepted: 16 May 2021 •
Published Online: 7 June 2021

View Online Export Citation CrossMark

Yinxu Bian,[1] Yannan Jiang,[2] Weijie Deng,[3,4] Renbing Shen,[2] Hua Shen,[1,5,a)] and Cuifang Kuang[6,7,a)]

AFFILIATIONS

[1] School of Electronic and Optical Engineering, Nanjing University of Science and Technology, Nanjing 210094, China
[2] Department of General Surgery, The Affiliated Suzhou Hospital of Nanjing Medical University, Suzhou Municipal Hospital, Suzhou 215002, China
[3] Changchun Institute of Optics, Fine Mechanics and Physics, Chinese Academy of Sciences, Changchun 130033, China
[4] Key Laboratory of Optical System Advanced Manufacturing Technology, Chinese Academy of Sciences, Changchun 130033, China
[5] Department of Material Science and Engineering, University of California, Los Angeles, Los Angeles, California 90095, USA
[6] State Key Laboratory of Modern Optical Instrumentation, Zhejiang University, Hangzhou 310027, China
[7] College of Optical Science and Engineering, Zhejiang University, Hangzhou 310027, China

[a)] **Authors to whom correspondence should be addressed:** edward_bayun@163.com and cfkuang@zju.edu.cn

ABSTRACT

Singlet microscopy is very attractive for the development of cost-effective and portable microscopes. In contrast to conventional microscope objectives, which consist of multiple lenses, the manufacturing process for singlet lenses is done without extensive assembling and aligning. In this manuscript, we report a novel singlet virtual Zernike phase contrast microscopy setup for unstained pathological tumor tissue slides. In this setup, the objective consists of only one lens. There is no need for the inset Zernike phase plate, which is even more expensive than a whole brightfield microscopy setup. The Zernike phase contrast is virtually achieved by the deep learning computational imaging method. For the practical virtual Zernike phase contrast microscopy setup, the computational time is less than 100 ms, which is far less than that of other computational quantitative phase imaging algorithms. With a conceptual demo experimental setup, we proved our proposed method to be competitive with a research-level conventional Zernike phase contrast microscope and effective for the unstained transparent pathological tumor tissue slides. It is believed that our deep learning singlet virtual phase contrast microscopy is potential for the development of low-cost and portable microscopes and benefits resource-limited areas.

INTRODUCTION

In contrast to conventional microscope objectives, which consist of multiple lenses, the manufacturing process of singlet lenses is done without precise assembling and testing.[1–6] Thus, singlet microscopy setups are very potential for low-cost and portable microscopes, which are very useful in resource-limited areas and Internet mobile medicine. In addition, in conventional brightfield microscopy, the pathological tissue slices and cells are usually chemically dyed. Chemical dyeing and fluorescent labeling are very attractive to medical and biological researchers, as details of tissues/cells are labeled as different colors. Under basic brightfield microscopes, these color differences are observed easily. However, on one hand, chemical dyeing and fluorescent labeling would make the tissues and cells inactive. On the other hand, they also require many resources, including time, reagent, precise instruments, and labor. To overcome these problems, phase imaging microscopy[7–11] is used for observing biological tissues and cells *in vitro*. Without chemical dyeing and fluorescent labeling, transparent and weakly scattering biological tissues/cells are imaged as the relative/quantitative phase information distribution. Conventional phase contrast microscopes consist of extensive, precise, and clean optical elements, which limits their usage in the research-level clean room, such as Zernike phase contrast (ZPC) microscopes,

quantitative phase imaging (QPI) microscopes, and Michelson interferometer holography microscopes. Recently reported quantitative phase imaging (QPI) microscopy methods,[7,8] e.g., Fourier ptychographic microscopy (FPM),[9,10] ptychographical iterative engine (PIE),[12] and deep learning methods,[8,11] have simple and robust configurations. With less computational time and multiple images, deep learning microscopy for transparent undyed bio-samples[8,13–15] shows superiorities over other computational methods.

In this manuscript, we propose to combine an aspheric singlet lens and the deep learning computational imaging method to construct a novel singlet phase contrast microscopy setup. In this setup, the circular quasi-monochromatic illumination part provides oblique propagation light, instead of brightfield illumination. A singlet microscope objective lens is custom-designed by ourselves. The field-of-view (FOV) of this designed singlet lens is competitive with those of the commercial same-magnification microscope objectives. In addition, the singlet lens has perfect linear-signal-transfer properties, which requires the same signal modulation transfer function (MTF) across the wide FOV. The pathological tissue slices/cells would be placed at the objective plane, and the CMOS image sensor is at the conjugate focal plane in the imaging space to record the digital image. After digital recording, the oblique illuminated image would be transferred into the ZPC microscope using our deep learning computational imaging algorithm. In the following, first, the principle and description about our singlet virtual ZPC microscopy setup are given. Second, the description, designing, and manufacturing information about the linearly signal-transferring singlet lens are presented. Third, details about the virtual ZPC imaging deep learning convolution network are provided. Finally, the experimental results, data analysis, and discussions are presented.

SINGLET VIRTUAL ZPC MICROSCOPY

Figure 1 shows the hardware schematic of our deep learning singlet virtual ZPC microscopy setup. In Fig. 1(a), a conventional ZPC microscope[16] is simplified. Quasi-chromatic light emits from a light source, which could be a traditional halogen lamp or a light emitting diode (LED) chip. The light would be condensed by a designed optical structure, e.g., Kohler illumination. Then, the light passes through an annular stop. After the annular stop, there is another condenser lens. The annular stop is at the front focal plane of this condenser. The pathological slide is placed at the back focal plane of this condenser. The structural and transmission information is modulated onto the optical wavefront, which includes phase retardation and diffraction. Most unstained/unlabeled thin pathological tissue slices are transparent. The background light is very strong, which would depress the efficient diffracted signal light. Thus, under a novel bright-field microscope objective lens, the efficient diffracted signal light would not be observed clearly. However, in the ZPC microscopy setup, as shown in Fig. 1(a), a Zernike phase plate is added at the Fourier spectrum plane. The Zernike phase plate and the annular stop are usually designed as a pair. Focusing with a tube lens, the ZPC microscopy image would be clearly recorded with a digital CCD/CMOS image sensor. In this manuscript, we propose a singlet objective lens to achieve a virtual ZPC microscopy

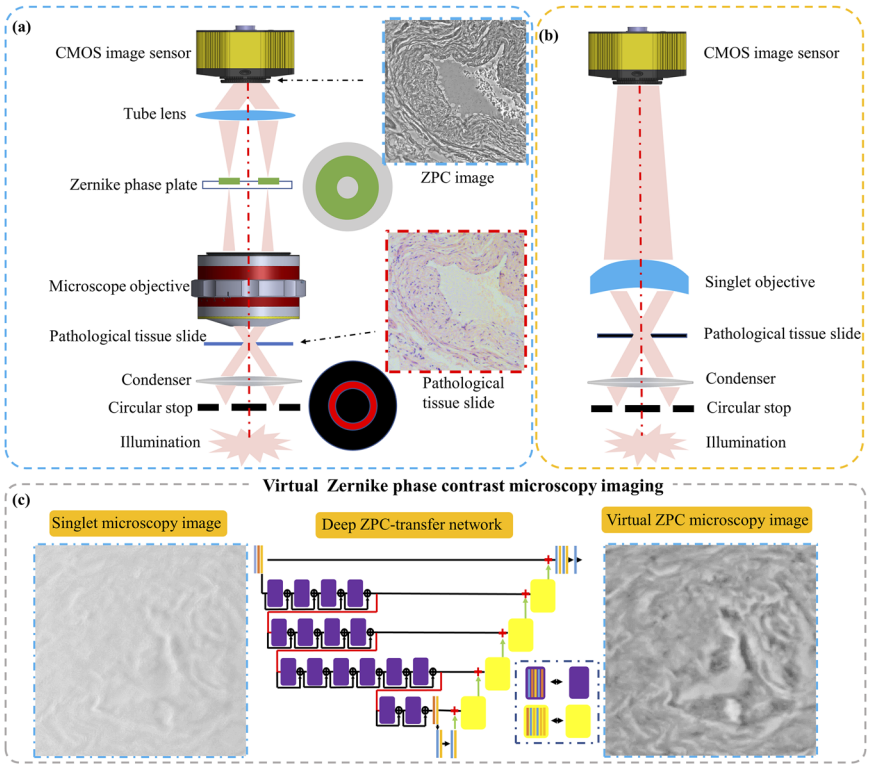

FIG. 1. Schematic of our deep learning singlet virtual ZPC microscopy setup: (a) conventional ZPC microscope, (b) proposed singlet microscope under circular illumination, and (c) deep learning framework to achieve virtual ZPC microscopy imaging.

setup based on the deep learning computational imaging method, whose hardware structure is illustrated in Fig. 1(b). The circular illumination part is still Kohler illumination modulated by an annular stop. However, instead of conventional microscope objectives consisting of multiple lenses, we use a customized aspheric singlet lens here. Our singlet lens is designed as a 4×-magnification imaging lens with a finite conjugate imaging length. The pathological tissue slide is at the objective plane, while a digital CMOS image sensor is at the conjugate imaging plane. By comparison, it is found that the optical structure in Fig. 1(b) is far more cost-effective and simpler than that in Fig. 1(a). However, only with the optical hardware in Fig. 1(b), we could not obtain a ZPC microscopy image of the transparent pathological tissue slice. We need to computationally process the directly recorded image by the deep learning ZPC-transfer method. In Fig. 1(c), the "using stage" of our singlet virtual ZPC microscopy setup is presented. Before the "using stage," the ZPC-transfer deep neural network (DNN) kernel would be deeply trained in the "training stage," which would be described in detail in the section titled Virtual deep ZPC-transfer. When the digital CMOS image senor records an image, this image would be convoluted with the ZPC-transfer DNN kernel. Then, the visual contrast of the microscopy image would be improved. The above method is named as deep learning singlet virtual phase contrast microscopy.

SINGLET MICROSCOPY OBJECTIVE LENS

In an imaging system, the normalized modulation transfer function (NMTF) could quantitatively describe the signal transferring abilities.[17–20] The spatial resolution ability is commonly limited by the imaging system's cut-off spatial frequency. Here, we designed and manufactured an aspheric singlet lens with the finite conjugate imaging length. When designing, we inversed the imaging system, where the CMOS image sensor is viewed as the objective plane and the pathological tissue slide is viewed as the imaging plane, shown in Fig. 2(a). The FOV in the space of the pathological tissue slide is ±2.5 mm. The numerical aperture (NA) in the space of the pathological tissue slide is 0.1. The effective focal length is 10 mm. The manufactured aspherical lens is shown in Fig. 2(b). The surface data are expressed as the mathematic polynomial of the high order even aspherical surface[20] as follows:

$$Z = \frac{cr^2}{1+\sqrt{1-(1+k)c^2r^2}} + \alpha_1 r^2 + \alpha_2 r^4 + \cdots + \alpha_8 r^{16}, \quad (1)$$

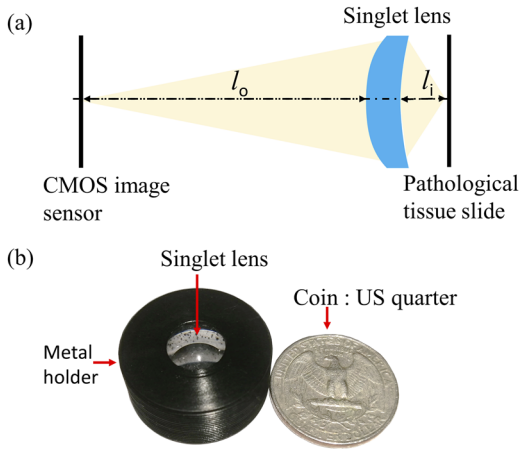

FIG. 2. Singlet microscopy objective lens: (a) schematic of inverse optics designing and (b) photograph of our aspheric singlet lens.

where c is the curvature ($1/R$), k is the aspheric coefficient, and α is the high order term coefficient. Even aspherical parameters S1 and S2 are presented in Table I.

In conclusion, our designed aspherical singlet lens has a high cut-off spatial frequency in the pathological tissue slide space, which is 350 lp/mm, under the quasi-chromatic illumination. The lens maintained almost the same NMTFs across the FOV of (−2.5, 2.5 mm), which would strengthen the performance of point-of-function (PSF) deconvolution algorithms and virtual deep ZPC-transfer algorithms.

VIRTUAL DEEP ZPC-TRANSFER

There are two stages in the singlet virtual deep ZPC-transfer computational microscopy method, as shown in Fig. 3: the "training stage" [Fig. 3(a)] and the "using stage" [Fig. 3(b)]. In the "training stage," two data stacks of unregistered images are input to the DNN to train the parameters. One of the image data stacks is the PSF-deconvoluted singlet microscopy images, named as DA in Fig. 3(a). The other is the commercial research-level ZPC microscopy images under a 4×-magnification standard objective (0.12 NA), named as DB in Fig. 3(a). In the "using stage," after the ZPC-transfer DNN kernel parameters are trained, the input singlet images are convoluted with the trained ZPC-transfer DNN kernel. Then, the output image is the desired virtual ZPC microscopy image. The "training

TABLE I. Even aspherical parameters (S1 and S2).

	R	k	α_2	α_3
S1	8.244	−1	1.986×10^{-4}	8.481×10^{-5}
S2	11.117	−1	6.557×10^{-4}	-3.289×10^{-5}
α_4	α_5	α_6	α_7	α_8
-7.485×10^{-7}	4.82×10^{-8}	-1.564×10^{-9}	2.142×10^{-11}	-5.421×10^{-14}
9.938×10^{-6}	1.37×10^{-7}	-2.272×10^{-7}	2.235×10^{-8}	-6.649×10^{-10}

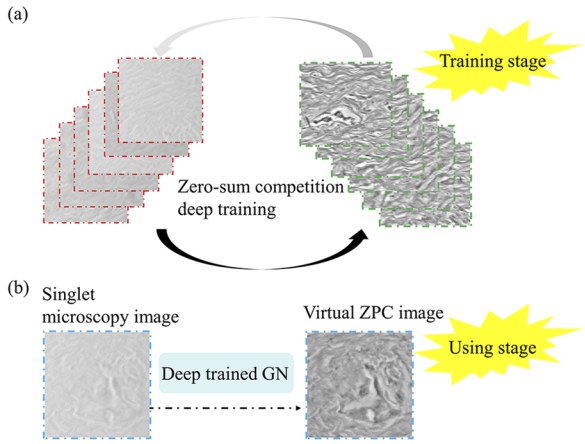

FIG. 3. Two stages in the proposed deep learning virtual ZPC imaging for singlet microscopy: (a) training stage to obtain a deep ZPC-transfer network by a zero-sum competition deep computational training and (b) using stage to transfer the singlet image to a virtual ZPC image.

stage" is very important to obtain the ZPC-transfer DNN kernel parameters mapping the singlet circular illumination microscopy image with the ZPC microscopy image, which is presented in Fig. 4.

As shown in Fig. 4, a ZPC-transfer DNN based on the generative adversarial network (GAN)[21–27] is adopted for virtual singlet ZPC microscopy imaging. There are two training cycles to go on a zero-sum competition.[21–24] The framework seems a Taiji (or the Great Ultimate), which would combine two different things into a united harmony. Here, the "two different things" are the singlet circular illumination microscopy image stack and the conventional Zernike phase contrast microscopy image stack. In the generator GN1:S to Z, the singlet circular illumination microscopy images are the input data. The aim of GN1:S to Z is to create "fake data," i.e., a "fake" ZPC-style image. Approximately, the aim of GN1:Z to S is to create "fake data," i.e., a "fake" circular illumination microscopy image, where the input data are the ZPC microscopy image. For the generator networks of Cycle 1 and Cycle 2, they have their own discriminator networks (DNs). Specifically, Discriminator Z aims to distinguish the "fake" ZPC-style image from the "real" conventional ZPC microscopy image, and Discriminator S aims to distinguish the "fake" singlet (S) image from the "real" singlet (S) microscopy image. In our deep ZPC-transfer DNN, digital image registration algorithms are not necessary. Thus, although the singlet circular illumination microscopy image stack and the conventional ZPC microscopy image stack are recorded using different digital CMOS cameras, there are no processes about computational imaging rotation, registration, and rescaling. To combine the singlet circular illumination microscopy image stack and the conventional ZPC microscopy image stack into a united harmony like a Taiji (or the Great Ultimate), we also design the following loss function:

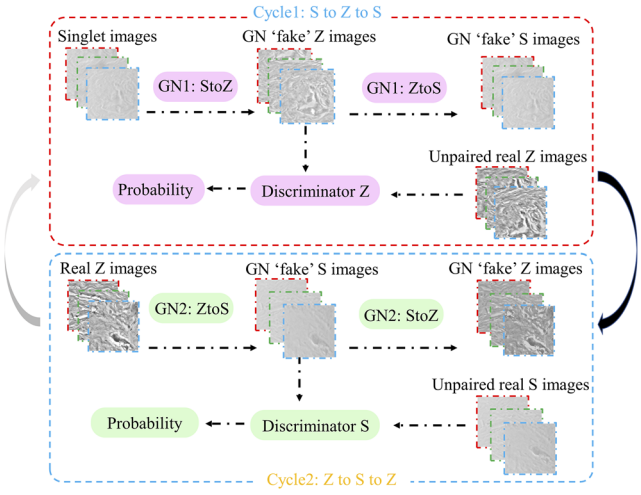

FIG. 4. Framework to train a deep ZPC-transfer network.

$$\begin{aligned} Loss = {} & L(GN1 : S\ to\ Z) + L(GN2 : Z\ to\ S) \\ & + L(cycle) + 0.1(1 - msSSIM(GN1, Z)) \\ & + 0.1(1 - msSSIM(GN2, S)), \end{aligned} \tag{2}$$

where $L(GN1 : S\ to\ Z)$ and $L(GN2 : Z\ to\ S)$ are the loss functions for each couple of GN-DN. $L(cycle)$ is the total cycle consistency loss. The last two terms are to maintain the image texture and structural information.[22,23] In brief, the loss function, i.e., Eq. (2), should aim to reserve the color and feature information.

MATERIAL

The raw material of our singlet is E48R (ZEON Corp, JAPAN). The lens was obtained from the Nanjing University of Science and Technology (NJUST). For both high-order even aspherical surfaces, their root-mean-square (rms) surface errors are controlled better than $\lambda/3$, where the optical shop testing wavelength is (λ = 632 nm). To maintain good coaxiality, the centration error between the two aspheric surfaces should be better than 1 arc min. Both surface qualities, which describe flaws, dust, and so on, should be better than 60/30 scratch/dig. The root-mean-square roughness of both aspheric surfaces should be better than 5 nm. The quasi-monochromatic illumination LED is a green LED with the power of 3 W. The pathological tissue slide is held on a 3D printed plastic structure. The 3D printed plastic structure is fixed on a 3D-axial adjuster (XR25C/M, ZHISHUN, China). The resolution of this 3D-axial adjuster is better than 10 μm. It is a green LED, which is at the dominant wavelength of 532 nm with the spectrum width of ~20 nm (FHWM). The working power is 3 W. The commercial Zernike phase contrast microscope, which consists of a digital CMOS image sensor, is NIB900L (NOVEL, Ningbo, China). The digital CMOS image sensor in the singlet microscopy setup is from HIKVISION, Hangzhou, China (MV-CE200-10GM). The pathological tissue slide is biologically and chemically processed in the medical lab of Suzhou Municipal Hospital (SMH). The pathological tissues are from human tumor tissues, which are sliced into standard sections (~2 to 4 μm thickness). These tumor tissues are following de-identification of the basic clinical information, which is supervised by the Medical and Biological Ethical Committee of the SMH. After slicing, these thin sections

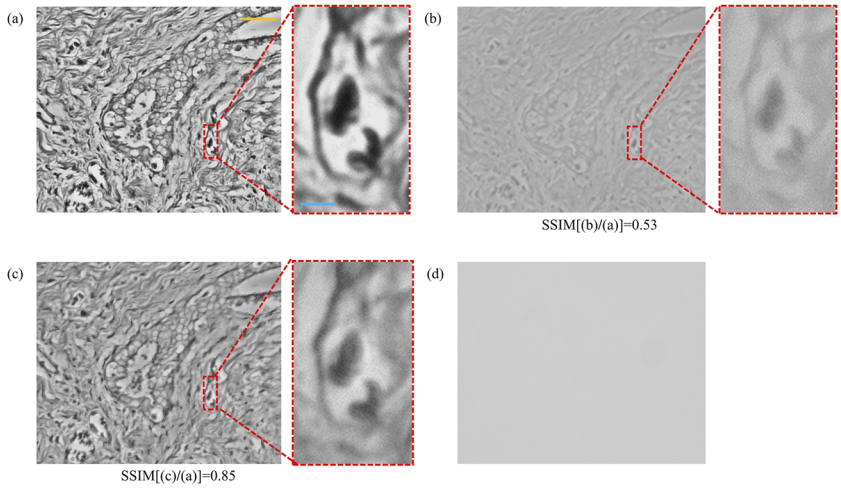

FIG. 5. Virtual ZPC imaging example for singlet microscopy. (a) ZPC image captured using the conventional ZPC microscope. The yellow scalar bar is ~100 μm. The blue scalar bar is ~20 μm. (b) Deconvoluted image captured using by our singlet microscope. (c) Virtual ZPC image based on the deconvoluted singlet microscopy image captured by our deep learning method. (d) Image captured using the brightfield microscope.

would be baked for half an hour at 68 °C. This process is to prevent falling. Afterward, these sections are deparaffinized with xylene and distilled water by 95% alcohols. Finally, the pathological tissue slides are sealed with neutral resin gum and a coverslip glass. For deep training a ZPC-transfer DNN kernel, our training process is executed using Python 3.7 and TensorFlow framework version 2.1. About the computational hardware, we use a bench-top computer, which is mainly equipped with a Core i7-7700K central processing unit (CPU) (Intel), 64GB of RAM (Kingston), and a piece of NVIDA GPU module, i.e., GeForce GTX 1080Ti GPU module.

EXPERIMENTAL DATA

In the singlet microscopy experimental setup, first, a stack of grayscale images is recorded under the annular illumination of the green LED by the digital CMOS image sensor. Second, the same set of unstained pathological tissue slides is placed under the commercial microscope objective with the same magnification. The ZPC microscopy images are also recorded. It is not necessary to record the same areas of the pathological tissue slides in these two recording processes. Third, the singlet microscopy images are deep learning deconvoluted for a higher image contrast. Fourth, the images are all cropped into the digital size of 512 * 512 pixel^2. Finally, the cropped images are executed to train the deep learning ZPC-style transferring process as illustrated in the section titled Virtual deep ZPC-transfer. For training, we used 2048 unpaired image couples, and for testing, we used 256 unpaired image couples. In the network framework, the batch size is 4, the learning rate is 0.0002, and the epochs are 10 000.

Figure 5 shows experimental data comparison, where the unstained pathological sliced tumor tissue slide is adopted as a transparent bio-sample. Figure 5(a) shows the "real" ZPC image captured using the conventional ZPC microscope. Figure 5(b) shows the singlet image under quasi-chromatic circular illumination. Figure 5(c) shows the virtual ZPC image based on the deep learning computational imaging method. Figure 5(d) shows the conventional brightfield microscopy image. From the vision comparison of Figs. 5(b) and 5(c), it is found that that the image contrast is improved much. From the quantitative data comparison, the SSIM between Figs. 5(b) and 5(a) is 0.53, while the SSIM between Figs. 5(c) and 5(a) is improved up to 0.85.

CONCLUSION

In this manuscript, we constructed the simplest ZPC microscopy setup among all known ZPC microscopes. Our simplest ZPC microscopy setup is based on two highlights. One is our designed aspherical singlet objective, which is free from extensive assembling and aligning, and the other is the deep learning ZPC computational imaging method. This means that there is no need for the inset Zernike phase plate in our singlet microscopy setup. For the practical virtual phase contrast microscopy setup, the computational time is less than 100 ms, which is far less than that of other computational quantitative phase imaging algorithms. Through imaging, deep training, and data comparison, it is shown that our methods are effective for transparent undyed sliced pathological tumor tissue slides. Our deep learning transfer methods are also fit for other rapid phase imaging methods, e.g., transport-of-intensity-equation (TIE),[28] PIE,[29] and FPM.[30,31] We believe that our deep learning singlet virtual phase contrast microscopy offers the potential for the development of low-cost and portable microscopes and benefits resource-limited areas.

ACKNOWLEDGMENTS

This study was partially supported by the National Natural Science Foundation of China (NSFC) (Grant No. 62005120), the Basic Research Program of Jiangsu Province (Grant Nos. BK20190456 and BK20201305), the Fundamental Research Funds for the Central Universities (Grant No. 30919011261), the Beijing Satellite Environmental Engineering Institute (Grant No. CAST-BISEE2019-038), the Chinese Academy of Sciences (No. KLOMT190101), the Suzhou Science and Technology Development Project (Grant No. SYSD2020132), and the National Key Research and Development Program (Grant No. 2019YFB2005500).

All authors declare that they have no conflict of interest.

DATA AVAILABILITY

The data that support the findings of this study are available from the corresponding authors upon reasonable request.

REFERENCES

[1] G. Muyo, A. Singh, M. Andersson, D. Huckridge, A. Wood, and A. R. Harvey, Opt. Express **17**(23), 21118 (2009).
[2] F. Languy, K. Fleury, C. Lenaerts, J. Loicq, D. Regaert, T. Thibert, and S. Habraken, Opt. Express **19**(S3), A280 (2011).
[3] R. G. González-Acuña and H. A. Chaparro-Romo, Appl. Opt. **57**(31), 9341 (2018).
[4] J. Nagar, S. D. Campbell, and D. H. Werner, Optica **5**(2), 99 (2018).
[5] J. Chen, J. Rao, D. Lisevych, and Z. Fan, Appl. Phys. Lett. **114**(10), 104101 (2019).
[6] X. Wan, W. X. Jiang, H. F. Ma, and T. J. Cui, Appl. Phys. Lett. **104**(15), 151601 (2014).
[7] Y. Ohene, I. Marinov, L. de Laulanié, C. Dupuy, B. Wattelier, and S. Starikovskaia, "Phase imaging microscopy for the diagnostics of plasma-cell interaction," Appl. Phys. Lett. **106**, 233703 (2015).
[8] J. K. Zhang, Y. R. He, N. Sobh, and G. Popescu, APL Photonics **5**(4), 040805 (2020).
[9] A. Pan, Z. Chao, X. Yuege, L. Ming, and Y. Baoli, Opt. Lasers Eng. **120**, 40 (2019).
[10] A. Pan, C. Zuo, and B. Yao, Rep. Prog. Phys. **83**(9), 096101 (2020).
[11] J. Zhu, R. Zhou, L. Zhang, B. Ge, C. Luo, and L. L. Goddard, Opt. Express **27**(5), 6719 (2019).
[12] J. Dou, Z. Gao, J. Ma, C. Yuan, Z. Yang, D. Claus, and T. Zhang, Appl. Phys. B **123**(8), 217 (2017).
[13] Y. Rivenson, Y. Zhang, H. Günaydın, D. Teng, and A. Ozcan, Light: Sci. Appl. **7**(2), 17141 (2018).
[14] Y. Rivenson, T. Liu, Z. Wei, Y. Zhang, K. de Haan, and A. Ozcan, Light: Sci. Appl. **8**(1), 23 (2019).
[15] Y. Rivenson, K. de Haan, W. Dean Wallace, and A. Ozcan, BME Front. **2020**, 9647163.
[16] C. S. Yelleswarapu, S.-R. Kothapalli, F. J. Aranda, D. V. G. L. N. Rao, Y. R. Vaillancourt, and B. R. Kimball, Appl. Phys. Lett. **89**(21), 211116 (2006).
[17] Y. Peng, Q. Sun, X. Dun, G. Wetzstein, W. Heidrich, and F. Heide, ACM Trans. Graphics **38**(6), 219 (2019).
[18] X. Dun, H. Ikoma, G. Wetzstein, Z. Wang, X. Cheng, and Y. Peng, Optica **7**(8), 913 (2020).
[19] H. Shen and J. Gao, J. Biophotonics **13**(6), e202000013 (2020).
[20] Y. Bian, Y. Jiang, Y. Huang, X. Yang, W. Deng, H. Shen, R. Shen, and C. Kuang, APL Photonics **6**, 031301 (2021).
[21] K. de Haan, Y. Rivenson, Y. Wu, and A. Ozcan, Proc. IEEE **108**(1), 30 (2020).
[22] H. Liang, K. N. Plataniotis, and X. Li, arXiv:2007.12578 (2020).
[23] D. Mahapatra, B. Bozorgtabar, J.-P. Thiran, and L. Shao, arXiv:2008.02101 (2020).
[24] H. Nishar, N. Chavanke, and N. Singhal, arXiv:2010.02659 (2020).
[25] S. Montresor, M. Tahon, A. Laurent, and P. Picart, APL Photonics **5**(3), 030802 (2020).
[26] J. Qian, S. Feng, T. Tao, Y. Hu, Y. Li, Q. Chen, and C. Zuo, APL Photonics **5**(4), 046105 (2020).
[27] S. Ren, Y. Luo, T. Yan, L. Wang, D. Chen, and X. Chen, AIP Adv. **11**, 015029 (2021).
[28] Y. Bian, Y. Zhang, P. Yin, H. Li, and A. Ozcan, Opt. Express **26**(23), 29614 (2018).
[29] J. Dou, J. Wu, Y. Zhang, Y. Hu, and Z. Yang, Opt. Express **28**(3), 3587 (2020).
[30] A. Pan, C. Zuo, Y. Xie, M. Lei, and B. Yao, "Vignetting effect in Fourier ptychographic microscopy," Opt. Lasers Eng. **120**, 40–48 (2019).
[31] A. Pan, K. Wen, and B. Yao, "Linear space-variant optical cryptosystem via Fourier ptychography," Opt. Lett. **44**(8), 2032–2035 (2019).